THE ASTROPHYSICAL JOURNAL, 595:L77–L80, 2003 October 1

FIRST GAMMA-RAY IMAGES OF A SOLAR FLARE

G. J. HURFORD,[1] R. A. SCHWARTZ,[2] S. KRUCKER,[1] R. P. LIN,[1,3] D. M. SMITH,[1,4] AND N. VILMER[5]

Received 2003 April 18; accepted 2003 July 3; published 2003 September 8

ABSTRACT

Imaging of gamma-ray lines, produced by nuclear collisions of energetic ions with the solar atmosphere, provides the only direct indication of the spatial properties of accelerated ions near the Sun. We present the first gamma-ray images of a solar flare, obtained with the *Reuven Ramaty High Energy Solar Spectroscopic Imager* (*RHESSI*) for the X4.8 flare of 2002 July 23. Two rotating modulation collimators (with 35″ and 183″ resolution) were used to obtain images for the same time interval in four energy bands: the narrow deuterium line at 2.223 MeV formed by the thermalization and capture of neutrons produced in the collisions; the 3.25–6.5 MeV band that includes the prompt de-excitation lines of C and O; and the 0.3–0.5 and 0.7–1.4 MeV bands that are dominated by electron bremsstrahlung. The centroid of the 2.223 MeV image was found to be displaced by $20'' \pm 6''$ from that of the 0.3–0.5 MeV image, implying a difference in acceleration and/or propagation between the accelerated electron and ion populations near the Sun.

Subject headings: gamma rays: observations — Sun: flares — Sun: X-rays, gamma rays

1. INTRODUCTION

Radio and hard X-ray observations have long been used to study energetic electrons accelerated near the Sun (e.g., Aschwanden 2002). In addition to exploiting detailed timing and spectral signatures, these observations also use high-resolution imaging with a few arcseconds resolution to locate the accelerated electrons in the context of the solar magnetic fields that govern their propagation.

The corresponding acceleration of ions to high energies in large solar flares has been established by the detection of nuclear gamma-ray line emission (e.g., Chupp 1990). Ions and electrons are also accelerated at higher altitudes of $\sim(2–40)R_s$ (Kahler 1994), most likely by shock waves driven by fast coronal mass ejections (CMEs), as indicated by studies of solar energetic particle (SEP) events at 1 AU.

When energetic ions collide with the solar atmosphere, they produce excited nuclei that emit prompt nuclear de-excitation lines, as well as secondary neutrons and positrons that result in the delayed 2.223 MeV neutron-capture and 511 keV positron-annihilation line emission (Ramaty & Murphy 1987). Spectral observations have provided information on the energy spectrum of the accelerated ions and on the composition of the ambient atmosphere and the accelerated ions (e.g., Chupp 1984; Share & Murphy 1995). In most events, the time profile of the prompt gamma-ray line emission is observed to be very similar to that of the bremsstrahlung hard X-rays emitted by energetic electrons, suggesting that the acceleration and propagation of the flare-accelerated ions and electrons are closely related. In contrast to the case of accelerated electrons, however, the location, size, and geometry of the ion collision regions remain unknown since, until now, the required imaging at energies above ~100 keV has not been available. This Letter presents the first gamma-ray images of a solar flare and so provides the first direct indication of where the accelerated ion population is located at the Sun.

2. OBSERVATIONS

The NASA *Reuven Ramaty High Energy Solar Spectroscopic Imager* (*RHESSI*) mission is designed for flare X-ray/gamma-ray imaging spectroscopy from 3 keV to 17 MeV (Lin et al. 2002). It observed the X4.8 flare of 2002 July 23, optically centered near the east limb at S13°, E72° (see Lin et al. 2003 for an overview of the observations).

The *RHESSI* imaging system consists of nine bi-grid rotating modulation collimators (RMCs) that provide FWHM angular resolutions from 2.″26 to 183″ in logarithmically spaced steps. Behind each RMC is an electrically segmented germanium detector (GeD), cryogenically cooled to provide high spectral resolution (~1–10 keV FWHM). The intense fluxes of low-energy (~3–250 keV) X-rays from strong flares stop primarily in the ~1 cm thick front segment, allowing ≥0.25 MeV gamma rays to be detected in the ~7 cm thick rear segment without significant dead time (Smith et al. 2002).

As the spacecraft rotates, the fraction of the incident flux that passes through the two grids in each RMC varies rapidly. Information on the location and morphology of the source is encoded in the timing of the photons that are detected after passing through both grids (Hurford et al. 2002). The time- and energy-tagged counts, together with aspect data, allow us to reconstruct and place the image on the solar disk. Here we use the rear-segment counts for RMCs 6 (35.″3) and 9 (183″). Their 2 and 3 cm thick tungsten grids modulate effectively at gamma-ray energies (see Table 1 for RMC parameters). For this flare, the aspect sensors (Zehnder et al. 2003; Hurford & Curtis 2002) provided positional accuracy of better than 2″.

Figure 1 shows rear-segment background-subtracted count rates versus time in the 0.3–0.5, 0.7–1.4, 2.218–2.228, and 3.25–6.5 MeV bands, summed over eight GeDs (excluding GeD 2, which was not segmented). Detector backgrounds were estimated from spectral accumulations on previous and subsequent days (± 15 orbits) when the spacecraft passed over similar geographic locations (Smith et al. 2003). The background ranged from ~50% of the average counting rates in the

[1] Space Sciences Laboratory, University of California at Berkeley, 7 Gauss Way, Berkeley CA 94720-7450; ghurford@ssl.berkeley.edu, krucker@ssl.berkeley.edu, rlin@ssl.berkeley.edu.

[2] NASA Goddard Space Flight Center, Science Systems and Application, Inc., Greenbelt, MD 20771; richard.schwartz@gsfc.nasa.gov.

[3] Department of Physics, University of California at Berkeley, 366 LeConte Hall, Berkeley, CA 94720-7300.

[4] Now at the Department of Physics and Santa Cruz Institute for Particle Physics, University of California at Santa Cruz, 1156 High Street, Santa Cruz, CA 95064.

[5] LESIA, Observatoire de Paris, 5 Place Jules Janssen, 92195 Meudon Cedex, France; nicole.vilmer@obspm.fr.

TABLE 1
IMAGING PARAMETERS AND RESULTS

Item	RMCs	300–500 keV	700–1400 keV	2218–2228 keV	3250–6500 keV
Total counts in map	6, 9	17819, 17126	13082, 12226	194, 130	2885, 2677
Source/total counts (%)	9	23	15	>89	31
Grid-pair transmission[a]	6, 9	0.24, 0.23	0.33, 0.26	0.43, 0.30	0.45, 0.31
Modulation amplitude[a,b]	6, 9	0.76, 0.81	0.46, 0.71	0.24, 0.53	0.22, 0.50
Photopeak efficiency[c]	6, 9	0.23, 0.22	0.16, 0.15	0.100, 0.095	0.046, 0.045
Imaged flux (photons cm^{-2} s^{-1})	9	4.7 ± 0.3	2.8 ± 0.3	0.30 ± 0.06	3.5 ± 0.6
	6	2.5 ± 0.3	1.6 ± 0.4	0.28 ± 0.12	…
Relative visibility	6/9	0.54 ± 0.06	0.57 ± 0.16	0.93 ± 0.43	…
Centroid offset (arcsec)[d]	6+9	874, 235	875, 238	875, 255	…
Location error (arcsec)	6+9	±2	±4	±6	…

[a] Rotationally averaged.
[b] Instrumental parameter (=0.81 for ideal, thin, opaque grids with equal slits and slats).
[c] Individual rear segments.
[d] Heliocentric east, south of Sun center.

flare interval at 0.3–0.5 MeV to ~70% in 0.7–1.4 and 3.25–6.5 MeV bands, not including the flare-generated background. All the images in this Letter are made for the same time interval, 00:27:20–00:34:40 UT, corresponding to the most intense impulsive peak. (Although lending additional support to the conclusions drawn below, discussion of the 2.223 MeV emission after this time interval is deferred to a later paper.)

The background-subtracted gamma-ray count spectrum from 0.3 to 8.5 MeV (Lin et al. 2003) was fitted to a model that includes the prompt nuclear de-excitation lines (including the α-α lines), the 2.223 MeV neutron-capture line, the 0.511 MeV positron-annihilation line, and a broken power-law electron-bremsstrahlung continuum. All were folded through the full instrument response, including off-diagonal terms from photons that deposit only part of their energy in the detector (Smith et al. 2002). The best fit indicates that the 0.3–0.5 and 0.7–1.4 MeV bands are dominated by the electron-bremsstrahlung continuum with ~12% and ~20%, respectively, of the background-subtracted counts due to the nuclear component (mostly nuclear photons that leave only part of their energy in the GeD). The C and O nuclear line complex accounts for ~60% of the 3.25–6.5 MeV band, with the rest from the electron-bremsstrahlung continuum.

Fast neutrons from energetic ion collisions thermalize in the photosphere before being captured by hydrogen to form deuterium, which then emits a 2.223 MeV photon. This results in a very narrow line with an intrinsic width of ≤0.1 keV, delayed by ~100 s. *RHESSI* detects this line with high resolution (~4 keV FWHM; Murphy et al. 2003), so a narrow energy band (2.218–2.228 MeV) can be used for imaging. This minimizes the underlying continuum background and non-photopeak response.

Figure 2 shows low-resolution (183″) gamma-ray images made with the back-projection technique (Hurford et al. 2002)

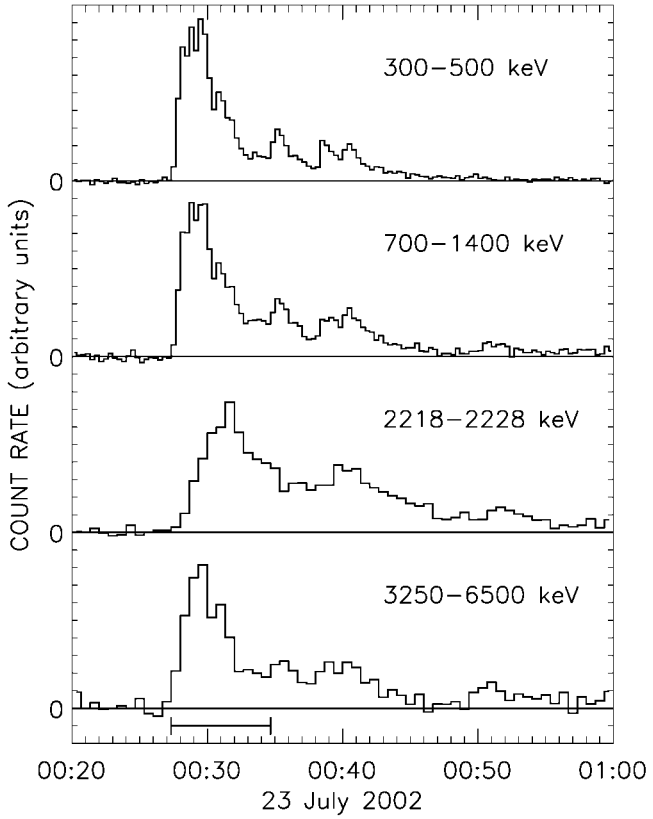

FIG. 1.—Background-subtracted light curves at the four imaged gamma-ray energy bands. Time resolutions are 20, 20, 40, and 40 s, respectively. The time interval used for mapping (00:27:20–00:34:40 UT) is shown at the bottom.

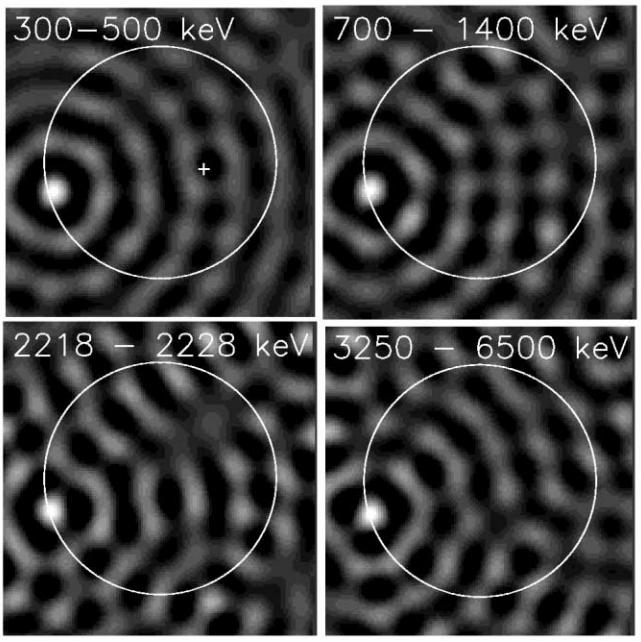

FIG. 2.—Low-resolution (183″ FWHM) "dirty" maps at four gamma-ray energies. The 2218–2228 keV map was made with a total of only 130 counts. The gray scale is linear with negative sidelobes suppressed. The circle represents the solar disk with heliocentric north and west at the top and right, respectively. *RHESSI* was rotating about a spin axis indicated by the plus sign with a period of 4.084 s.

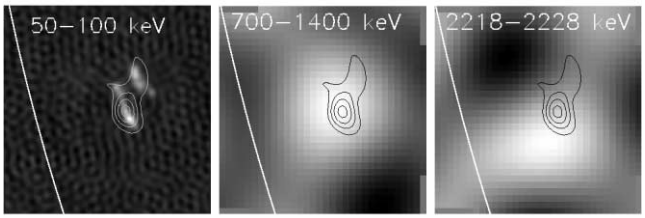

FIG. 3.—Each panel shows the same 300–500 keV ~7″ resolution "CLEANed" map as 30%, 50%, 70%, and 90% contours. The fields of view are 96″ × 96″, centered 880″ east and 240″ south of Sun center with a white arc indicating the solar limb. The left panel compares these contours to a high-resolution (3″), front-segment hard X-ray map at 50–100 keV. The middle and right panels show expanded gray-scale views of the central peak of 35″ resolution dirty maps in the 700–1400 keV and 2218–2228 keV bands, respectively. Although the sources are not resolved with this resolution, it is apparent that the centroids of emission at these two bands are displaced from one another.

using RMC 9 only. These represent a convolution of the source and the RMC beam with its characteristic circular sidelobes. This beam is circularly symmetric with the radial profile given by the zero-order Bessel function, $J_0(\pi r/R)$, where R is the FWHM resolution. The main peaks show unambiguously that the gamma-ray sources are related to the optical flare at S13°, W72°.

Intermediate-resolution (35″) maps (Fig. 3) made by summing back-projection images from RMCs 6 and 9 show a significant southerly displacement of the 2.218–2.228 MeV peak with respect to the 0.7–1.4 MeV peak. The corresponding map at 3.25–6.5 MeV did not reveal a significant peak. Photons of these energies are particularly susceptible to forward scattering from the 2 cm thick lower grid of RMC 6, an effect that lowers the effective modulation amplitude below the nominal value shown in Table 1.

Figure 4 shows the RMC 6+9 peak locations for the 0.3–0.5, 0.7–1.4, and 2.218–2.228 MeV bands as circles with radii equal to the 1 σ statistical error [$\sigma = 2RN^{0.5}/(\pi aS)$, where a is the modulation amplitude and N is the total number of counts of which S represents the source counts]. Since the imaging parameters are identical for the different energy bands, errors in aspect solution, dead-time corrections, grid parameterization, or the role of finite angular resolution, etc., are common. Thus their effects on relative source locations are discounted.

Attempts at imaging the solar 511 keV line were limited by the strong background line at that energy and yielded only a 3 σ upper limit of 0.7 photons s^{-1} cm^{-2} between 506 and 516 keV, consistent with the spatially integrated 511 keV line flux reported by Share et al. (2003).

3. DISCUSSION OF RESULTS

The images at 2.218–2.228 and 3.25–6.5 MeV provide our first indication of the spatial distribution of the accelerated ions near the Sun. The fact that we were able to image these sources with collimator resolutions of 35″ and 183″, respectively, implies that the sources are not large and diffuse on these size scales.

The gamma-ray images made with resolutions of 35″ and 183″ show fully unresolved (e.g., consistent with a point source) or partially unresolved single-component images with no statistically significant evidence of a noncircular source shape on these size scales. For such images, information is limited to the centroid of the emission and the imaged flux. The centroid is defined as the peak of the convolution of the real (unknown) source distribution with the 35″ Bessel function beam specified above. If the real source structure is asymmetrical or contains

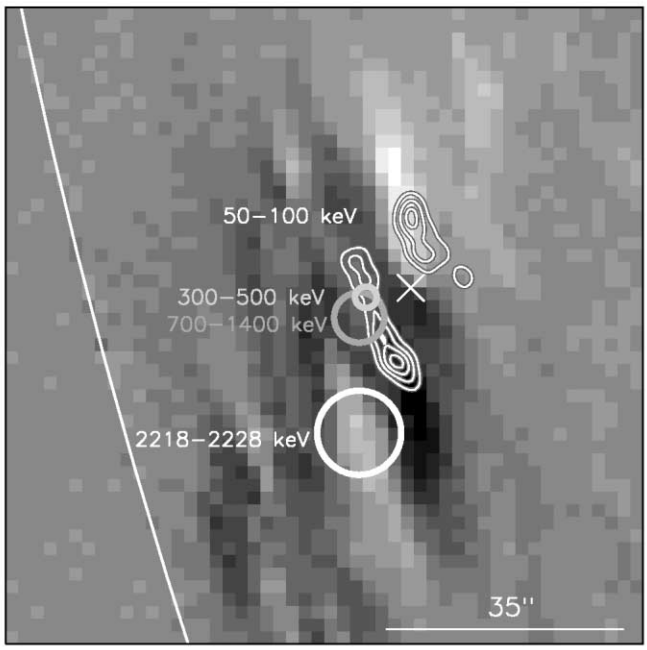

FIG. 4.—Locations of the gamma-ray sources. The thick circles represent the 1 σ errors for the 300–500 keV (*light gray*), 700–1400 keV (*dark gray*), and 2218–2228 keV (*white*) maps made with identical parameters. The 35″ FWHM angular resolution is shown in the lower right. The field of view is the same as in Fig. 3. The white contours show the high-resolution 50–100 keV map with 3″ resolution. The cross shows the centroid of the 50–100 keV emission made with the same lower resolution as the gamma-ray maps. The background image is a *SOHO*/MDI magnetogram acquired at 00:12 UT, 15 minutes prior to the flare.

significant flux at low surface brightness, this low-resolution centroid may not necessarily coincide with the peak of a map made with higher resolution. However, if two maps made with the same resolution have significantly different peaks, their spatial distributions *must* be different.

For RMC images made by the back-projection algorithm, the expectation values of the peak intensity (and its location) are independent of background. The magnitude of the imaged flux is the flux of a point source that would give rise to the same peak intensity. For an unresolved source, the imaged flux is the spatially integrated flux.

For the 0.3–0.5 and 0.7–1.4 MeV bands, the imaged flux with 35″ resolution was significantly less than that obtained with 183″ resolution. The ratios of the imaged flux with RMC 6 to that with RMC 9—0.54 ± 0.06 and 0.57 ± 0.16, respectively—are defined as the relative visibilities (Table 1). The fact that these are not unity indicates that the sources were partially resolved on a size scale of 35″.

The 0.3–0.5 and 0.7–1.4 MeV images are consistent, in terms of both their relative visibilities and their centroid locations (which differed by 3.″0 ± 8.″8). We therefore have no indication that the source structure or location at 0.3–0.5 MeV differs from that at 0.7–1.4 MeV.

There is some evidence, however, that the 0.3–0.5 MeV image differs from that at hard X-ray energies. At 0.3–0.5 MeV, RMCs 3–7 were used to make a higher resolution (~7″) map (see the contours in Fig. 3) with a "CLEAN" algorithm. Figures 3 and 4 also show a high-resolution (3″) 50–100 keV hard X-ray image made with the front segments of RMCs 1–7. A string of compact hard X-ray sources extends ~24″ along a north-south direction, with a second, ~12″ long parallel string located ~10″ closer to Sun center (see Krucker, Hurford, & Lin 2003,

Emslie et al. 2003, and White et al. 2003). The 0.3–0.5 MeV contours (Fig. 3) overlap the east string, with the lowest intensity contour also extending to the west string. This suggests that the east string is relatively more intense at higher energies. This difference between the X-ray and gamma-ray electron-bremsstrahlung images is confirmed by the fact that the 50–100 keV hard X-ray centroid, obtained with RMCs 6 and 9 as for the other bands, is displaced ~8″ west of the centroids of the 0.3–0.5 and 0.7–1.4 MeV emission (Fig. 4).

For the nuclear component, the relative visibility of the 2.223 MeV line source was 0.93 ± 0.43. This is consistent both with that of the 0.3–0.5 and 0.7–1.4 MeV image morphology discussed above and with a value of unity, which would suggest a compact source. If we take 0.07 as a 2 σ lower limit to the relative visibility and make an arbitrary (but simple) assumption of a "Gaussian model," this would imply a 2 σ upper limit to the 2.223 MeV source size of ~1′ FWHM.

The time history of the 2.223 MeV line emission has been fitted to a detailed physical model (Hua, Ramaty, & Lingenfelter 1989; Hua et al. 2002) that includes energy losses, magnetic mirroring, and pitch-angle scattering in a loop with an active region atmosphere (Murphy et al. 2003). The neutron production time history is assumed to be given by the prompt nuclear de-excitation line flux, as measured by the 4–7.6 MeV band. The accelerated ions interact in the lower chromosphere/upper photosphere to produce the fast neutrons and prompt de-excitation lines, while the neutron thermalization and capture on hydrogen occurs close by, within ~500 km, in the photosphere (R. J. Murphy 2003, private communication). Thus, the 2.223 MeV line emission region helps us to locate the energetic ion interaction region to within 1″.

The 2.223 MeV source centroid was found to be displaced in the southward direction from the weighted average of the 0.3–0.5 and 0.7–1.4 MeV sources by $20'' \pm 6''$, which is nonzero with a statistical confidence of greater than 99.7%. Since the 0.3–0.5 and 0.7–1.4 MeV bands are partially (~12%–20%) contaminated by the nuclear gamma-ray counts, this is an underestimate of the actual displacement of the sources characteristic of the electrons and of the ions. Although the real source structures are unresolved, this displacement implies that there are significant differences in location and/or morphology between the electron- and ion-associated sources.

In the vicinity of the 2.223 MeV centroid, no significant hard X-ray emission is detected; all the hard X-ray sources are north and toward Sun center. No flare Hα or radio emission is observed at the centroid either, although weak Hα emission is seen both to the east and to the west.

A previous insight into the spatial properties of the accelerated ions was provided by the detection of the 2.223 MeV line from the behind-the-limb flare of 1989 September 29 (Vestrand & Forrest 1993). This suggested that either some acceleration occurs far from the optical flare or the accelerated ions were transported over large distances. In contrast to this event, that flare had an associated large SEP event observed at 1 AU. In that case, some of the SEPs accelerated by the fast CMEs may have precipitated into the solar atmosphere to produce neutrons and the 2.223 MeV line emission. In such a situation, the 2.223 MeV source would not necessarily be compact as was observed here.

To within ~10 s, the time profiles of the 0.3–0.5 and 0.7–1.4 MeV count rates (dominated by electron bremsstrahlung) are generally similar to that of the 3.25–6.5 MeV nuclear prompt line emission (Fig. 1). This similarity has been seen in other gamma-ray flares (Forrest & Chupp 1983) and has been interpreted as indicating a common acceleration process for electrons and ions. If electrons and ions are accelerated and transported similarly, however, the ion-associated gamma-ray source would be expected to coincide with the electron-bremsstrahlung source. One possibility is that DC electric field acceleration is involved. Then, the positively charged ions would be initially accelerated in the opposite direction from the electrons and could subsequently interact in spatially separated sources as observed here.

In summary, the first gamma-ray images of solar flares have shown that relativistic electron bremsstrahlung and the energetic ion sources are compact at the ~1′ level and are located close to the optical flare. The centroid of the ion source, however, is significantly displaced from the electron-bremsstrahlung source(s).

We thank M. Fivian for confirming the roll aspect solution, R. J. Murphy and G. H. Share for sharing results prior to publication, and B. R. Dennis and H. S. Hudson for their valuable comments. This work was supported by NASA grant NAS5-98033.

REFERENCES

Aschwanden, M. J. 2002, Space Sci. Rev., 101, 1
Chupp, E. L. 1984, ARA&A, 22, 359
———. 1990, Phys. Scr., T18, 15
Emslie, A. G., Kontar, E. P., Krucker, S., & Lin, R. P. 2003, ApJ, 595, L107
Forrest, D. J., & Chupp, E. L. 1983, Nature, 305, 291
Hua, X.-M., Kozlovsky, B., Lingenfelter, R. E., Ramaty, R., & Stupp, A. 2002, ApJS, 140, 563
Hua, X. -M., Ramaty, R., & Lingenfelter, R. E. 1989, ApJ, 341, 516
Hurford, G. J., & Curtis, D. W. 2002, Sol. Phys., 210, 101
Hurford, G. J., et al. 2002, Sol. Phys., 210, 61
Kahler, S. 1994, ApJ, 428, 837
Krucker, S., Hurford, G. J., & Lin, R. P. 2003, ApJ, 595, L103
Lin, R. P., et al. 2002, Sol. Phys., 210, 3
Lin, R. P., et al. 2003, ApJ, 595, L69
Murphy, R. J., Share, G. H., Hua, X.-M., Lin, R. P., Smith, D. M., & Schwartz, R. A. 2003, ApJ, 595, L93
Ramaty, R., & Murphy, R. J. 1987, Space Sci. Rev., 45, 213
Share, G. H., & Murphy, R. J. 1995, ApJ, 452, 933
Share, G. H., et al. 2003, ApJ, 595, L85
Smith, D. M., et al. 2002, Sol. Phys., 210, 33
Smith, D. M., Share, G. H., Murphy, R. J., Schwartz, R. A., Shih, A. Y., & Lin, R. P. 2003, ApJ, 595, L81
Vestrand, W. T., & Forrest, D. J. 1993, ApJ, 409, L69
White, S. M., Krucker, S., Shibasaki, K., Yokoyama, T., Shimojo, M., & Kundu, M. R. 2003, ApJ, 595, L111
Zehnder, A., et al. 2003, Proc. SPIE, 4853, 41